



High-Fidelity Finite Element Modeling of Wood-Sheathed Cold-Formed Steel Shear Walls

Fani Derveni, S.M.ASCE¹; Simos Gerasimidis, Ph.D., M.ASCE²; Benjamin W. Schafer, Ph.D., P.E., M.ASCE³; and Kara D. Peterman, Ph.D., M.ASCE⁴

Abstract: Cold-formed steel (CFS) framed construction has been widely adopted and used toward a modern, lightweight, and cost-efficient engineering practice across the United States. The primary objective of this work is to numerically assess the performance of CFS-framed shear walls sheathed with oriented strand board (OSB) and subjected to seismic events. A robust three-dimensional high-fidelity shell finite element model is developed and aims to provide a benchmark modeling approach able to accurately capture strength, stiffness, and failure mechanisms in these systems. Particular attention is given to the fundamental role of the connections between the CFS members and the OSB sheathing to the overall shear wall lateral response. To understand the variability in this critical connection, a series of 30 identical connection tests are performed. The robustness of the proposed computational model is validated by nine different CFS shear wall experimental studies and by a parametric analysis. The developed model is applied to provide an accurate experimentally-derived fastener-based computational tool of CFS-framed shear walls with potential use in design code expansion. DOI: 10.1061/(ASCE)ST.1943-541X.0002879.

© 2020 American Society of Civil Engineers.

Author keywords: Thin-walled structures; Cold-formed steel; Shear walls; Lateral loading; Computational modeling; Connection experiments.

Introduction

Cold-formed steel (CFS) framing has shown great escalation and potential in low- and midrise construction in the last 25 years due to the various benefits it offers. CFS structures offer a high strengthto-weight ratio, high durability, low-cost maintenance, noncombustibility, ease in installation, and prefabrication. This work focuses on the primary lateral force resisting system in CFS framing and specifically on the response of oriented strand board (OSB) sheathed CFS shear walls under earthquake demands. Typical CFS shear walls are constructed of CFS studs and CFS tracks composing the primary wall structural frame, which is sheathed with wood, steel, gypsum-based, or cement-based panels or braced by a strap. Hold-downs or tie-rods are used to prevent the uplift for these shear wall systems and details, such as connected distribution members, like ledgers, seams in the sheathing, blocking, and strapping (all may be present). CFS shear walls are governed by complex failure modes, and their response alters and varies depending on the selected components and details. OSB-sheathed CFS-framed shear

Note. This manuscript was submitted on February 26, 2020; approved on August 19, 2020; published online on November 20, 2020. Discussion period open until April 20, 2021; separate discussions must be submitted for individual papers. This paper is part of the *Journal of Structural Engineering*, © ASCE, ISSN 0733-9445.

walls have been approached by various research efforts through the system-, subsystem-, and connection-level testing and analysis.

CFS research at the full system level has been recently conducted as a part of the CFS-network for earthquake engineering simulation (NEES) project by focusing on a two-story building lateral behavior (Schafer et al. 2016). In particular, the OSB-sheathed CFS full-scale response exposed to earthquake events was examined by both experimental efforts (Peterman et al. 2016a, b) and computational efforts (Leng et al. 2013).

CFS subsystem shear wall research has been carried out by Santa Clara University, McGill University, and Johns Hopkins University by experimentally investigating the lateral response of CFS shear walls. In detail, the early work by Serrette (Serrette et al. 1996, 1997a, b, 2002) has assessed the lateral response of CFS shear walls sheathed with OSB, plywood, gypsum wallboard, and FiberBond wallboard and has been adopted by the North American Standard for OSB-sheathed CFS framed system provisions. Additionally, OSB-sheathed CFS shear walls have been extensively examined by Rogers (Branston 2004; Chen 2004; Blais 2006; Hikita 2006; Branston et al. 2006) by exploring the impact of various wall dimensions, different sheathing and steel thicknesses, and distinct fastener patterns under monotonic and reversed cyclic loading, aiming to enhance the North American design guidelines for light gauge construction. More recently, Schafer (Liu et al. 2012, 2014) has evaluated the effect of construction details, such as the impact of ledgers, OSB panel seams, field stud thickness, and interior gypsum presence in OSB-sheathed framed shear walls under monotonic and cyclic loading, targeting to advance the state of the art design provisions for those systems. In all of the aforementioned OSB-sheathed CFS shear wall tests, connections failures governed the full shear wall response and base shear capacity.

Various CFS subsystem shear wall modeling approaches have been introduced by multiple research works. Performance-based fastener-oriented computational investigations of OSB-sheathed CFS shear walls have been conducted via the Pinching4 material

¹Ph.D. Candidate, Dept. of Civil and Environmental Engineering, Univ. of Massachusetts Amherst, 130 Natural Resources Rd., Amherst, MA 01003 (corresponding author). ORCID: https://orcid.org/0000-0001-8159-0345. Email: fderveni@umass.edu

²Assistant Professor, Dept. of Civil and Environmental Engineering, Univ. of Massachusetts Amherst, 130 Natural Resources Rd., Amherst, MA 01003.

³Professor, Dept. of Civil and Systems Engineering, Johns Hopkins Univ., Latrobe Hall, 3400 N Charles St., Baltimore, MD 2128.

⁴Assistant Professor, Dept. of Civil and Environmental Engineering, Univ. of Massachusetts Amherst, 130 Natural Resources Rd., Amherst, MA 01003

in the OpenSees software environment (Buonopane et al. 2015; Bian et al. 2015; Kechidi and Bourahla 2016). Further numerical efforts of capturing a hysteretic wall response have been tackled through a complex spring representation by using DRAIN-3DX software (Fülöp and Dubina 2004) or through panel shell elements by using SAP2000 software and implementing a simplified finite element analysis (Martínez-Martínez and Xu 2011). Highfidelity finite element modeling efforts through the ABAQUS software have been performed (Ngo 2014; Ding 2015) with limited success and focused on specific CFS shear wall configurations and details. Although a variety of experimental studies has been conducted, along with various phenomenological performance-based modeling approaches, to the authors' knowledge, high-fidelity finite element methods able to capture the complex lateral response and failure modes of CFS shear walls for a variety of realistic structural configurations and details have not yet been reported.

Numerous studies have investigated the shear response of connections between CFS members and OSB sheathing. The influence of the sheathing type, CFS thickness, and fastener schedule was explored (Peterman et al. 2014) under monotonic and cyclic loading, while the impact of the sheathing type, thickness, and orientation along with steel thickness and strength was approached and tested (Okasha 2004). The effect of humidity conditions, overdriven fastener issues, edge distance, fastener spacing, and potential specimen reuse was also evaluated (Vieira and Schafer 2009, 2012) through monotonic testing. Different screw diameters, OSB and CFS thicknesses, and OSB orientations were explored (Iuorio et al. 2014) through a series of five or twelve identical repetitions of connection specimens, which concluded that fastener tilting and pull-through are the dominant connection failure mechanisms. Furthermore, a shear single-fastener response was examined by altering sheathing material in correlation with the fastener diameter and sheathing thickness (Moen et al. 2016), while sheathing types and orientation, fastener edge distances, and cyclic protocols and loading rates were varied (Fiorino et al. 2007, 2008). The connection response has also been evaluated by probabilistic approaches (Bian et al. 2017), and a further Monte Carlo simulation was used to address the connection impact on the overall shear wall response. Despite the wealth of experimental data, there are insufficient repetitions to form a robust statistical characterization of fastenersheathing behavior.

This work aims to provide a benchmark shear wall modeling approach for OSB-sheathed CFS shear walls under lateral loading. For this reason, a robust three-dimensional high-fidelity shell finite element model is introduced and validated by a set of nine recent and distinct CFS shear wall tests. The focal point of this work includes a fastener-based modeling approach similar to Buonopane et al. (2015) but augmented to better capture connection failure, including deformation from the sheathing and all steel components in the wall. To understand the variability in the connection response and provide accuracy in the introduced computational model, an aggregate of 30-specimen connection experiments is conducted. These tests not only benefit the modeling assumptions but also address the inherent variability of the connections between CFS members and OSB sheathing.

Experimental Characterization of CFS-to-OSB Connections

As connection behavior dominates the CFS-framed OSB-sheathed shear wall response, it is necessary to fully-characterize not only the strength, stiffness, and degradation, but the statistical variability of the shear connection response. The significance of this step lies in the CFS-to-OSB connection failure mechanism that governs the response of OSB-sheathed CFS shear wall systems. Thirty identical CFS-to-OSB connection tests were performed to ensure statistically significant results.

Test Setup and Test Specimen

The experimental setup consists of $304.8 \times 406.4 \,\mathrm{mm} \, (12 \times 16 \,\mathrm{in.})$ stud-screw-sheathing specimens subjected to monotonic loading. Two CFS studs are connected to two sheets of OSB sheathing on both sides via eight fasteners (Fig. 1). The test rig is adapted from Peterman et al. (2014). The web of the CFS studs is inserted between steel plates; the exterior steel plates are 25.4 mm (1 in.) thick, while the interior plates are 12.7 mm (1/2 in.) thick [Figs. 1(b and d)]. This aims to restrain the deformation of the web of the studs and to focus the failure into the fasteners in the flanges of the studs. The load is applied at the top of the rig and in a direction perpendicular to CFS stud flanges [as in Fiorino et al. (2007), Vieira and Schafer (2012), Peterman et al. (2014), and Iuorio et al. (2014)], while the bottom part is fixed. While a test setup in which load is parallel to the CFS stud flanges (Fiorino et al. 2017) mimics loading in a typical shear wall, load orientation is not expected to have an impact on the connection behavior due to the highly localized response.

The specimens are constructed of 1.37 mm (54 mils) thick CFS studs (lipped channel sections) of 152.4 mm deep web, 41.3 mm wide flange, and 12.7 mm deep lip {600S162-54 [AISI S200 12 (AISI 2012)]} connected to 11.11 mm (7/16 in.) thick, Exposure 1 OSB sheathing by M4 \times 50 (No. 8) flathead QuickDrive screws. In detail, 304.8 mm (12 in.) fastener spacing (s) is selected, and the fasteners are located at 38.1 mm (1.5 in.) from the edge of the sheathing to the center of the flanges of the studs, based on AISI S100 provisions [AISI S100-16 (AISI 2016)]. Finally, the edges of the screws were cut after installation to avoid fastener bearing on the stud web after tilting. This becomes necessary because of the excessive tilting of the fasteners during the tests, which is an unrealistic phenomenon in an actual shear wall response. In reality, the tilting of the screws in a CFS shear wall is parallel to the flange of the studs. Vieira and Schafer (2009) demonstrate that cutting the screw tips does not affect the connection response; this method was also successfully adopted by Peterman et al. (2014).

Test Results of 30 Identical Specimens

The force-displacement response of the 30 tests is shown in Fig. 2(a). As the load is not directed toward one side of the specimen or the other, all fasteners are free to fail first. The progression of failure is largely dependent on minute differences in installation, localized sheathing properties, and geometric imperfections. Observed failures were approximately random and followed no discernable pattern. Fasteners failed in either pull-through (21 out of 30 times), as pictured in Fig. 2(b) or shear (9 out of 30 times) as pictured in Fig. 2(c).

In the first case [Fig. 2(a)], tilting of the screws is observed at the beginning of the experiment, while the pull-through of the fasteners is initiated in some of the fasteners, followed by the local bearing of the sheathing around the screw location. This is a progressive failure mode, which is not accompanied by abrupt changes in a force-displacement response.

In the second case [Fig. 2(a)], the tilting of the fasteners is followed by abrupt drops in the force-displacement response representing a shear failure of the connections. In this failure mode, in tandem with the broken connections, fastener pull-through is

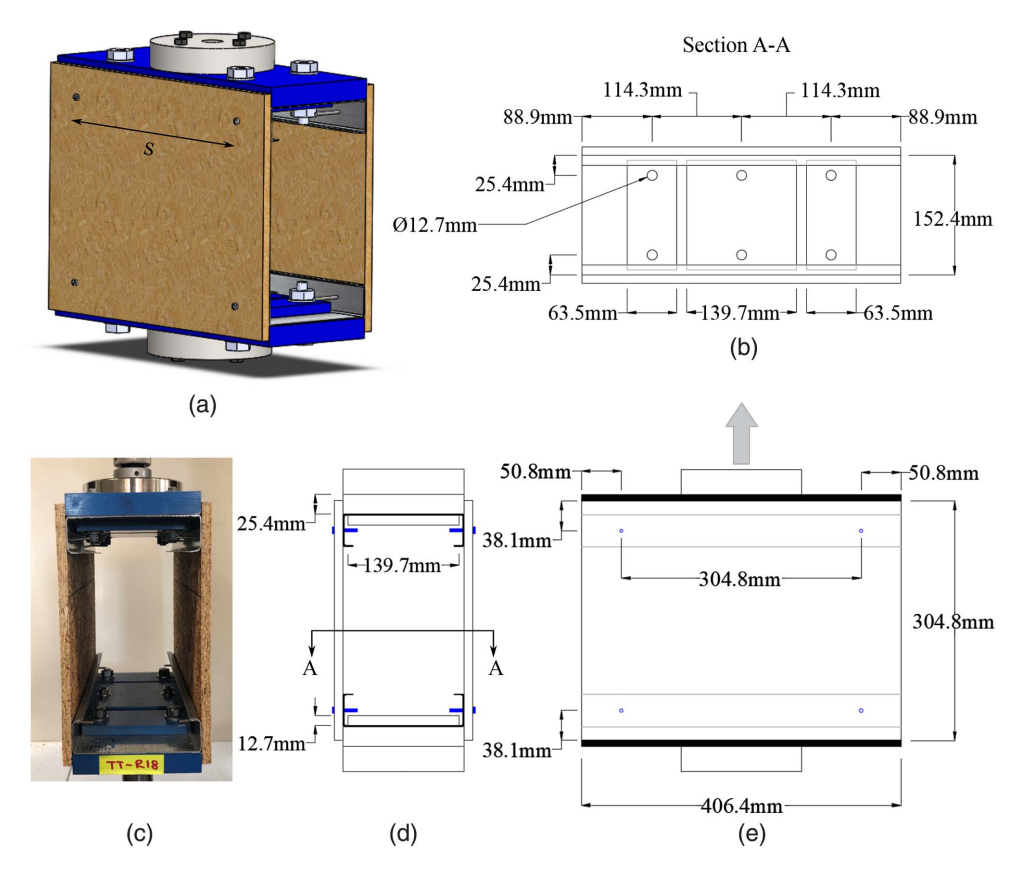


Fig. 1. Stud-screw-sheathing specimen and rig configuration: (a) isometric view of the specimen; (b) inside view of the specimen through Section A-A; (c) photo of actual test specimen; (d) side view of the specimen; and (e) front view of the specimen. Thirty identical specimens are tested by selecting a connection spacing of s = 304.8 mm.

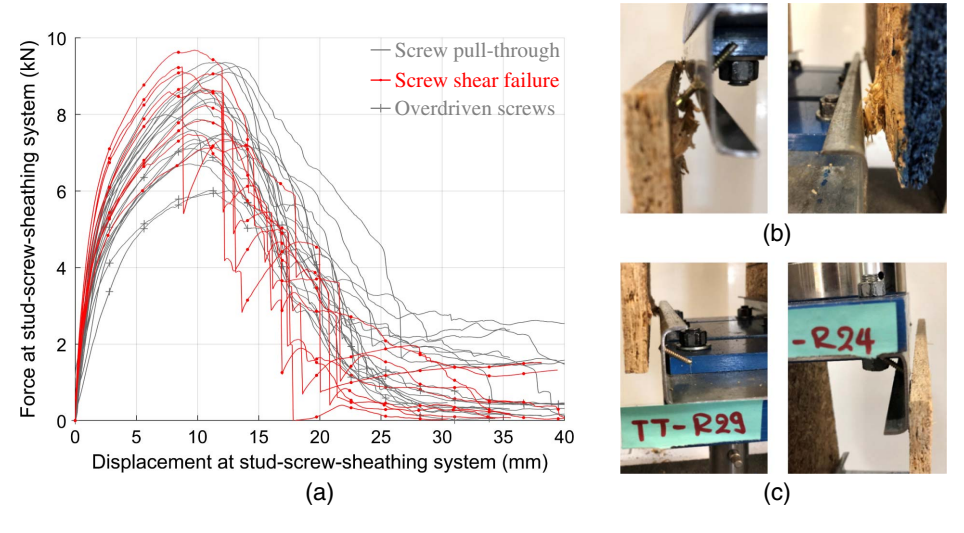


Fig. 2. Stud-screw-sheathing system experimental results under monotonic loading: (a) test results of 30 identical specimens. Pull-through and screw shear failure modes impact, as well as overdriven screws impact; (b) photos of actual screw pull-through failure mechanism after testing; and (c) photos of actual shear screw failure mechanism after testing.

also observed across the eight fasteners accompanied by the OSB localized bearing after the peak strength is reached.

Tensile coupon testing is also conducted for both CFS studs used in the specimens, which failed by abrupt shear failure [yield strength of 355 MPa (51 ksi)] and CFS studs used in pull-through governed specimens [yield strength of 332 MPa (48 ksi)]. In three of the specimens, one screw was overdriven (representing

approximately 1% of screws installed). In these instances, the screw was installed past the point of flushness with the OSB sheathing. These screws were subsequently backed out to align with the OSB board surface. These three specimens are identified in Fig. 2(a) with cross markers and represent some of the lower experimental strengths. This is consistent with past observations (Vieira and Schafer 2009), as overdriving the screw breaks the plane of the

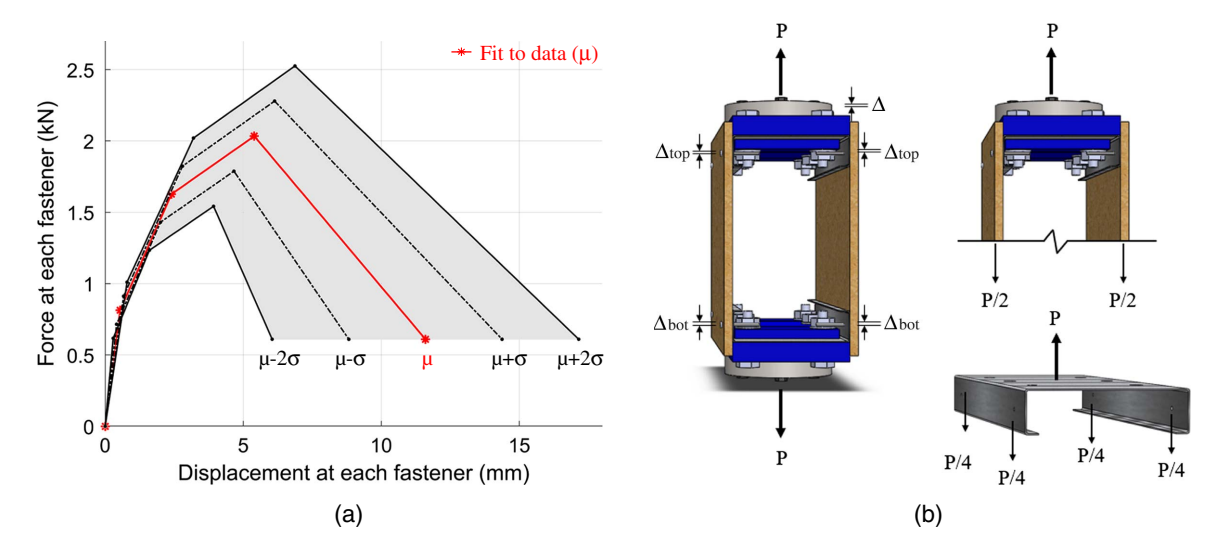


Fig. 3. Conversion of system response to individual fastener response and statistical connection characterization: (a) shear response enclosed by $\mu \pm \sigma$ bounds and $\mu \pm 2\sigma$ bounds. The fit-to-data line represents the statistical average response of the tests; and (b) displacement and force conversion per screw schematic representation.

sheathing and enables the fastener head to more easily burrow into the sheathing while bearing. Overdriven screws are relatively common in construction because of operator error, but due to their impact on connection strength, they are reported in this study.

A significant 38% variability on peak strength is observed in the examined 30-specimen sample. The high variability in the specimen response lies in the inherent fastener variance, as well as in the OSB material properties uncertainty.

Conversion to Single Screw Response

In order to move from the response of the system of eight fasteners (P is the system force, Δ is the system displacement, and K is the system stiffness) to the individual fastener response, a single screw force equation [Eq. (1)], a single screw stiffness equation [Eq. (2)], and a single screw displacement equation [Eq. (3)] are derived (Vieira and Schafer 2009) and are used in this study.

According to the free body diagram [Fig. 3(b)], the force per screw P_i is

$$P_i = P/4 \tag{1}$$

Based on a parallel spring model individual stiffness, K_i is calculated

$$K_i = K/2 \tag{2}$$

Due to the localized deformations in screw locations, individual fastener displacement Δ_i is defined

$$\Delta_i = \Delta/2 \tag{3}$$

A system to individual connection response conversion is selected in this study in order to enhance the effort of reducing

the connection response expected variability in comparison to the single-screw testing choice.

Statistical Characterization of Screw Response

The experimental study aims to a statistical characterization of a mean fastener shear response in order to address the variability in CFS connections. The average backbone of the 30 identical experiments is calculated based on the fit to data curve at a 40% peak load, 80% peak load, 100% peak load, and 30% postpeak load [Fig. 3(a)]. Mean values μ , standard deviations σ , and coefficients of variations COV of the four points constructing the backbone $(\Delta_i \text{ and } P_i)$ are calculated (Table 1). The mean backbone connection force-displacement response along with the bounds of $\mu \pm \sigma$ and $\mu \pm 2\sigma$ indicate the reliability range of the CFS-to-OSB connection response [Fig. 3(a)]. The coefficient of variation of the peak strength is 12%. Framing this within comparable experimental literature, COV is within the range reported by Iuorio et al. (2014), 6%–12%. It is notable that this work tested between 5 and 12 repetitions of CFS-to-OSB connections and used different specimen components and test setups in their experimental program, suggesting that the variation is relatively insensitive to these variables. Currently, there is not strength comparison for CFS-to-OSB screws in the design codes.

Numerical Modeling of Nine OSB Sheathed CFS Shear Walls

Finite element software ABAQUS is used (ABAQUS version 2014), and nine different experimental studies throughout the literature (Liu et al. 2014; Branston 2004; Blais 2006; Hikita 2006) are simulated for validation of the model for strength, stiffness, and failure mechanisms. The modeling approach developed is

Table 1. Statistical characterization parameters based on the aggregate of 30 identical connection experiments

Statistical quantity	$\Delta_1 \ (\text{mm})$	Δ_2 (mm)	Δ_3 (mm)	Δ_4 (mm)	P_1 (kN)	P_2 (kN)	P_3 (kN)	P_4 (kN)
Mean μ	0.54	2.40	5.40	11.6	0.81	1.63	2.03	0.61
COV (%)	23.30	16.70	13.80	24.00	12.10	12.10	12.10	12.10

Note: P_i denotes the load and Δ_i the displacement of the four points constructing the CFS-to-OSB connection behavior.

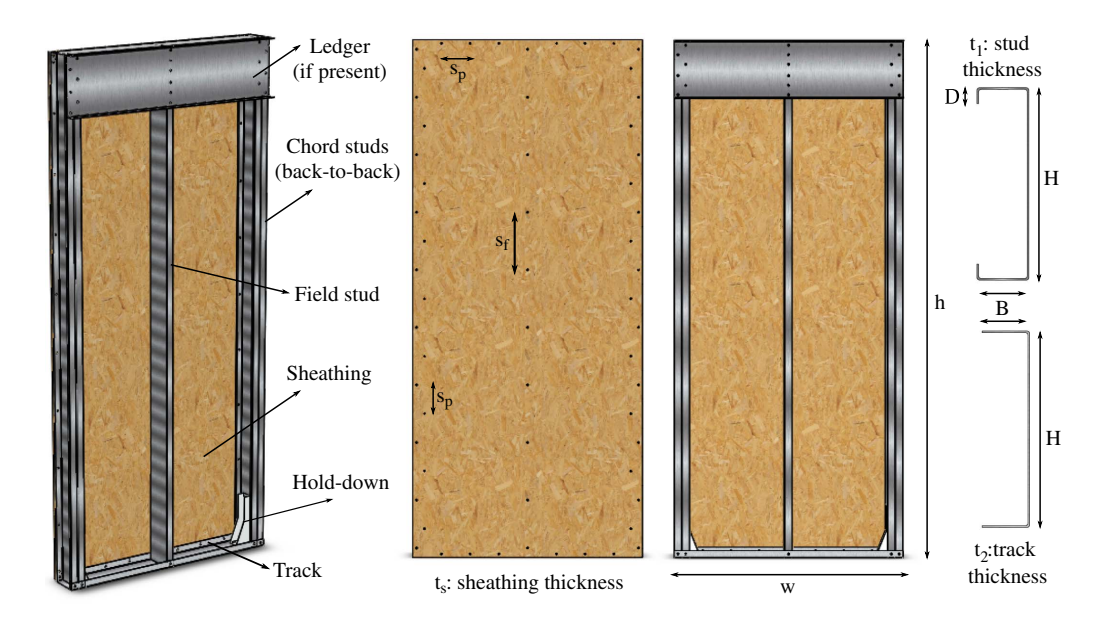


Fig. 4. Typical shear wall configuration representation, including wall dimension symbols and component cross-sectional dimension symbols. Nine shear wall configurations are simulated. In this study, h is the height of each wall, w is the width of each wall, s_p is the screw spacing at the shear wall perimeter, and s_f is the screw spacing at the shear wall field stud. For the cross-sectional dimensions notation, the symbol H is used for CFS stud and track web depth, B is used for CFS stud and track flange width, and D is used for the CFS stud lip depth, while t_1 represents the CFS stud thickness, t_2 represents the CFS track thickness, and t_s represents the OSB sheathing thickness.

employed consistently regardless of the wall configuration. The shear wall configurations modeled in this study are composed of back-to-back CFS chord studs, CFS field studs, and CFS tracks sheathed at the exterior sides with an OSB panel and connected to the foundation by hold-downs. Different details that exist in some of the selected walls are explained in the model geometry section. Experimentally-obtained CFS-to-OSB connection data are used for the simulation of the connections, which is the key point of this study.

Model Geometry

OSB-sheathed CFS shear walls simulated in this study differentiate from each other in multiple parameters, such as dimensions of the wall, cross-sections of studs and tracks, OSB sheathing thickness, CFS members thickness, hold-down components, and details, such as a ledger and vertical seam. The model geometry of the shear walls can loosely be classified into two categories based on the CFS-NEES work (Liu et al. 2014) and McGill's work (Branston 2004; Blais 2006; Hikita 2006).

In the case of Liu et al. (2014), two different wall configurations under monotonic loading are adopted in this study. The CFS structural frame is sheathed by OSB sheathing at the exterior side, while a ledger track is attached at the interior top side of the walls. Simpson Strong-Tie S/HDU6 (Dublin, California) hold-downs are used at the bottom part of the wall in order to prevent the wall uplift. The CFS components are connected by M5 (No. 10) screws, while the CFS members to OSB sheathing are connected by staggered M4 (No. 8) flathead Simpson Quick-Drive screws. In the case of the wall width (w) equal to 2.44 m (8 ft) in contrast to the wall width equal to 1.22 m (4 ft), a vertical seam is included in the middle field stud by two lines of connections in the stud flange spacing 152.4 mm (6 in.). Horizontal seams on OSB sheathing as well as residuals stresses and strains and geometric imperfections of CFS members are ignored in this model [as in Ngo (2014) and Ding (2015)] to

- reduce model complexity. In past experiments, CFS members did not buckle during the tests, indicating an insensitivity to residual stresses and imperfections in shear wall subsystems. Walls with horizontal seams behave as if the panel is continuous; they do not fail along the strap connecting the seam, and the horizontal seam location has little impact on the shear capacity of the wall (Liu et al. 2014).
- In the case of the McGill effort, seven shear walls under monotonic loading are adopted in this study (Branston 2004; Blais 2006; Hikita 2006). The structural frame is composed of CFS studs and tracks sheathed in the exterior by OSB sheathing. The OSB sheathing is attached to the CFS frame by M4 (No. 8) self-piercing screws examining three different spacing patterns in the perimeter of the sheathing at a 12.7-mm (1/2-in.) edge distance. Studs are fastened to tracks by M5 (No. 10) screws, while back-to-back chord studs are connected by M4 (No. 8) screws. Hold-downs are used at the bottom part of the walls, and specifically, the Simpson Strong-Tie S/HD10 model is selected in this case. Shear wall configurations and geometry are thoroughly illus-

trated by schematics of different typical CFS shear wall views (Fig. 4), including the basic symbols (see the "Notation" section) that are used for representing summarized component sections and details (Table 2), as well as compiled wall dimensions and basic differences between the simulated cases (Table 3).

Nominal dimensions and material properties are used for the nine-wall simulation with the purpose of introducing a generalized benchmark model.

Mesh Discretization

Shell elements are used for both CFS components and the OSB sheathing panel. Specifically, two-dimensional four-node shell elements (S4R) with reduced integration are chosen from the ABAQUS library. The extensive study by Schafer et al. (2010) emphasizes the high significance of the element type and mesh size in the behavior of the CFS members. In the current study, a fine mesh

Table 2. CFS cross-section details

Wall selection	Cross-section	H (mm)	B (mm)	D (mm)
Liu et al. (2014)	Stud (C-lipped)	152.40	41.3	12.7
	Track (C-unlipped)	157.40	38.1	_
	Ledger (C-unlipped)	304.80	50.8	_
Branston (2004)	Stud (C-lipped)	92.08	41.3	12.7
	Track (C-unlipped)	92.08	30.2	_
Blais (2006) and	Stud (C-lipped)	92.08	41.3	12.7
Hikita (2006)	Track (C-unlipped)	92.08	31.8	_

Note: H = CFS component web depth; B = CFS component flange width; and D = CFS stud-lip depth.

of a size of 6.35 mm (0.25 in.) is selected for the CFS members that allow for at least two elements in the lips of the studs, while a coarser mesh of a size of 50.8 mm (2 in.) is selected for OSB sheathing (Fig. 5). A finer mesh of 38.1 mm (1.5 in.) of OSB sheathing is also assessed in the parametric analysis section of this paper.

Material Properties

In this work, CFS components are modeled as elastoplastic isotropic materials, while OSB sheathing is simulated as an elastic orthotropic material.

CFS Material Simulation

For CFS members, an elastic-perfectly plastic material model is implemented with a modulus of elasticity $E=203~{\rm GPa}$ (29,500 ksi) and a Poisson's ratio v=0.3 in all of the examined configurations, while the perfectly plastic part is based on nominal yield strengths of 344 MPa (50 ksi) for the examined experimental studies by Liu et al. (2014) or 230 MPa (33 ksi) for the McGill-effort-investigated experimental works (Branston 2004; Blais 2006; Hikita 2006). Nominal yield strengths are used for generalizing the proposed finite element approach, while measured yield strengths are discussed subsequently in the parametric analysis section.

OSB Material Simulation

For OSB sheathing, the elastic orthotropic material properties are analytically calculated (Schafer et al. 2007) for both the 11.11 mm, 24/16 rated (7/16 in.) thick and 9.525 mm, 24/0 rated (3/8 in.) thick OSB sheathing. According to APA-D510C (APA 2012), the OSB panel bending stiffness $(EI)_s$ in both parallel to the strength axis $[(EI)_{s1};$ long panel direction] and perpendicular to the strength axis

 $[(EI)_{s2}]$, as well as the panel rigidity through the thickness $(Gt)_s$, are specified, and they are converted into the modulus of elasticity E_s [Eq. (4)] and shear modulus G_s [Eq. (5)], respectively.

The OSB panel modulus of elasticity is calculated

$$E_s = 12(EI)_s/t_s^3 \tag{4}$$

The OSB panel shear modulus is obtained

$$G_s = (Gt)_s/t_s \tag{5}$$

The summarized computed material properties (Table 4) are introduced to the finite element model for orthotropic materials from the ABAQUS library. Because orthotropic modeling requires material properties in three-dimensions, Young's modulus in the out-of-plane panel E_{s3} is assumed equal-to-perpendicular to the strength axis modulus of elasticity E_{s2} , and similarly, the out-of-plane shear modulus G_{s13} and G_{s23} are assumed to be equal to the in-plane shear modulus G_{s12} . The impact of the shear modulus is assessed in a parametric analysis section by examining the shear wall response by a set of different values. The Poisson's ratio is selected as $v_s = 0.3$ in all of the three-dimensions.

Connection Modeling

There are two types of connections modeled in this work. The first type is the connections between CFS members to OSB sheathing, and the second one is the connections between CFS members. Different modeling assumptions are introduced between the two types that are used in this model, based on their participation in the full shear wall response during the tests; CFS-to-OSB connections failed, but CFS-to-CFS connections did not fail.

CFS-to-OSB Connections

As CFS-to-OSB connections failure is observed to be the governing failure mechanism for OSB-sheathed CFS shear walls based on previous experimental studies (Liu et al. 2014; Branston 2004; Hikita 2006; Blais 2006), a fastener-based CFS shear wall approach is introduced. The connections are simulated through nonlinear connector element CONN3D2 Cartesian from the ABAQUS library that allows motion in the three translational degrees of freedom. Each connector element is composed of a wire of two nodes from which Node 1 is selected at the sheathing panel, while Node 2 is chosen on the CFS members [Fig. 5(b)].

Focusing on the two shear connection directions, available experimentally-determined data are introduced to represent each screw response. The assorted nonlinear connection behavior is

Table 3. Component and detail selection in all nine shear wall simulated configurations

					Space	cing	
Wall database (Test no.)	Wall, $w \times h$ (m)	OSB, t_s (mm)	Stud, t_1 (mm)	Track, t_2 (mm)	Perimeter, s_p (mm)	Field, s_f (mm)	Hold-down type
Liu et al. (2014) (1c)	1.22×2.74	11.110	1.37	1.37	152.4 ^a	304.8	S/HDU6
Liu et al. (2014) (11c)	2.44×2.74	11.110	1.37	1.37	152.4 ^a	304.8	S/HDU6
Hikita (2006) (51b)	1.22×2.44	11.110	1.37	1.09	152.4	304.8	S/HD10
Branston (2004) (21abc)	1.22×2.44	11.110	1.12	1.12	152.4	304.8	S/HD10
Branston (2004) (23abc)	1.22×2.44	11.110	1.12	1.12	101.6	304.8	S/HD10
Branston (2004) (25abc)	1.22×2.44	11.110	1.12	1.12	76.2	304.8	S/HD10
Blais (2006) (41abc)	1.22×2.44	9.525	1.09	1.09	152.4	304.8	S/HD10
Blais (2006) (43abc)	1.22×2.44	9.525	1.09	1.09	101.6	304.8	S/HD10
Blais (2006) (45abc)	1.22×2.44	9.525	1.09	1.09	76.2	304.8	S/HD10

Note: w = width of the wall; h = height of the wall; $t_s = \text{OSB thickness (out-to-out)}$; $t_1 = \text{stud thickness (out-to-out)}$; $t_2 = \text{track thickness (out-to-out)}$; $t_p = \text{screw spacing at wall perimeter}$; and $s_f = \text{screw spacing at wall field stud.}$

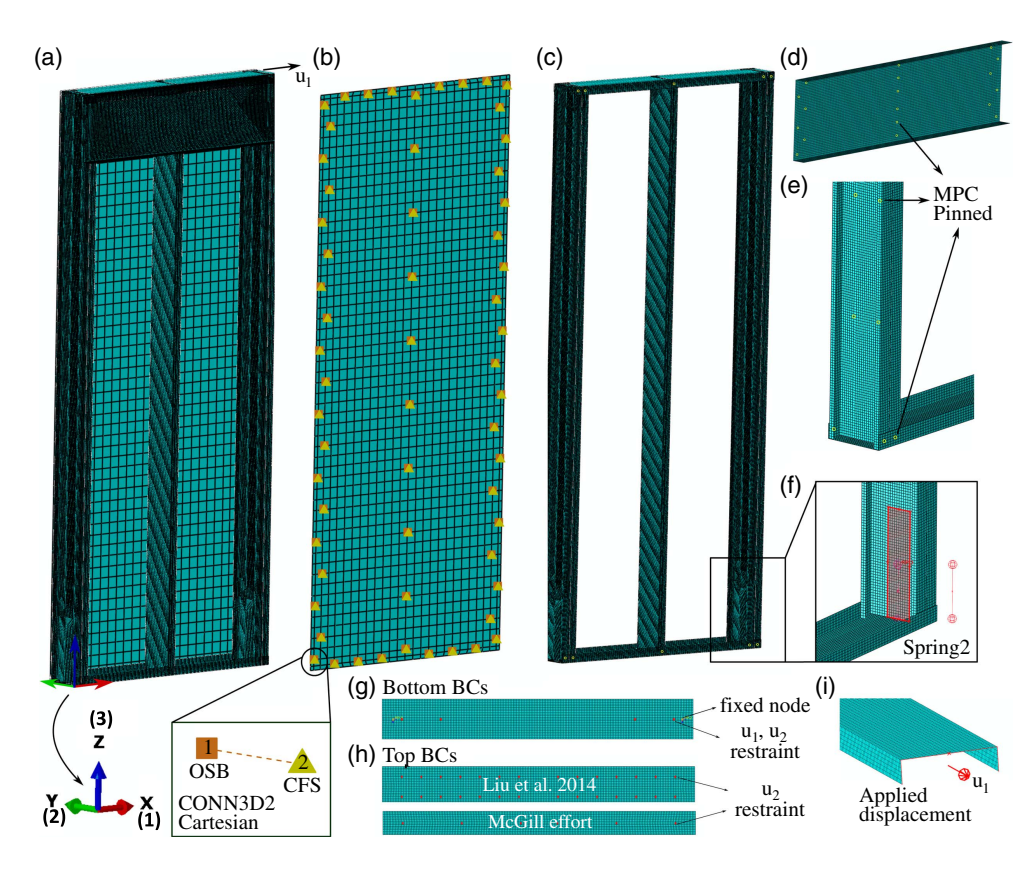


Fig. 5. Typical shear wall simulation representation for nine different wall specimens: (a) full-wall schematic indicating the model global coordinate system; (b) OSB sheathing mesh representation and CFS-to-OSB connection indication. The connector element Cartesian is used by selecting as a first node the OSB sheathing node and as a second node the CFS component node; (c) CFS structural frame composed of studs connected to tracks; (d) ledger simulation and mesh. The ledger is connected to CFS structural frame by MPC pinned constraints; (e) back-to-back CFS studs and studs to tracks are connected by MPC pinned constraints; (f) hold-down simulation by a rigid body connected to the foundation by a SPRING2 element; (g) boundary conditions at the bottom part of each wall; (h) boundary conditions at the top of the wall; and (i) applied monotonic displacement at the top track.

Table 4. OSB sheathing material properties

OSB sheathing type	$\frac{(EI)_{s1}}{(kN \cdot mm^2/mm)}$	$\frac{(EI)_{s2}}{(\text{kN} \cdot \text{mm}^2/\text{mm})}$	$\frac{(Gt)_{s12}}{(kN/mm)}$	E_{s1} (MPa)	E_{s2} (MPa)	G_{s12} (MPa)
11.11 mm, 24/16 rated	734.36	150.64	14.62	6,422	1,317	1,316
9.525 mm, 24/0 rated	564.90	103.56	13.57	7,844	1,438	1,425

Note: Modulus of elasticity and shear modulus are calculated based on the OSB thickness and rate of the different experimental configurations.

adopted based on the screw diameter and the thicknesses of the connected CFS and OSB materials. For this reason, four different connection backbones are implemented in the finite element tool with regards to each examined shear wall configuration: (1) 1.37 mm (54 mils) CFS to 11.11 mm (7/16 in.) OSB data by Peterman et al. (2014) for Liu et al. (2014) walls; (2) 1.37 mm (54 mils) CFS to 11.11 mm (7/16 in.) OSB connection data based on the backbone of the 30-test statistical average conducted in this study for the Hikita (2006) wall; (3) 1.12 mm (44 mils) CFS to 11.11 mm (7/16 in.) OSB behavior adopted by an estimated linear interpolation between the available 0.84 mm (33 mils) CFS and 1.37 mm (54 mils) CFS to 11.11 mm (7/16 in.) OSB tests by Peterman et al. (2014) for the Branston (2004) walls; and (4) 1.09 mm (43 mils) CFS to 9.525 mm (3/8 in.) OSB connection behavior based on an approximated strength reduction factor equal to the thickness difference between 9.525 mm (3/8 in.) and 11.11 mm (7/16 in.) OSB thickness for Blais (2006) walls. The connection backbones for the four different cases are summarized in Table 5 and are graphically illustrated in Fig. 6(a) with solid lines. It needs to be highlighted that besides the CFS-to-OSB nonlinear behavior selection, significant attention is also given to the orientation of those connections. In particular, the vector forces of CFS-to-OSB connections, mainly at the corners of the shear wall panels, are not aligned with one of the shear-direction axes of the global coordinate system [Fig. 6(b)]. For this purpose, it is very critical to introduce a local coordinate system at each fastener based on an average angle calculated by a former elastic analysis. Analytically, a two-stage analysis is implemented, as follows:

 Stage A: A linear elastic analysis is conducted for obtaining the CFS-to-OSB connections orientations. This means that geometric nonlinearities, material plasticity, and connection nonlinearities are eliminated, and the shear wall is subjected to monotonic

Table 5. Monotonic backbone CFS-to-OSB connection behavior

	Δ_1	Δ_2	Δ_3	Δ_4	P_1	P_2	P_3	P_4
CFS to OSB thickness pattern	(mm)	(mm)	(mm)	(mm)	(kN)	(kN)	(kN)	(kN)
1.37 mm CFS to 11.11 mm OSB ^a	0.576	3.301	6.846	10.76	0.879	1.742	2.178	0.653
1.37 mm CFS to 11.11 mm OSB ^b	0.540	2.400	5.400	11.60	0.814	1.627	2.034	0.610
1.12 mm CFS to 11.11 mm OSB	0.735	3.239	6.477	12.16	0.802	1.605	2.006	0.602
1.09 mm CFS to 9.525 mm OSB	0.735	3.239	6.477	12.16	0.682	1.364	1.705	0.512

Note: Symmetric response is in both tension and compression. The load-displacement $(P_i-\Delta_i)$ connection response is chosen based on CFS and OSB thicknesses of the different simulated wall configurations.

^bExperimentally-determined by this paper.

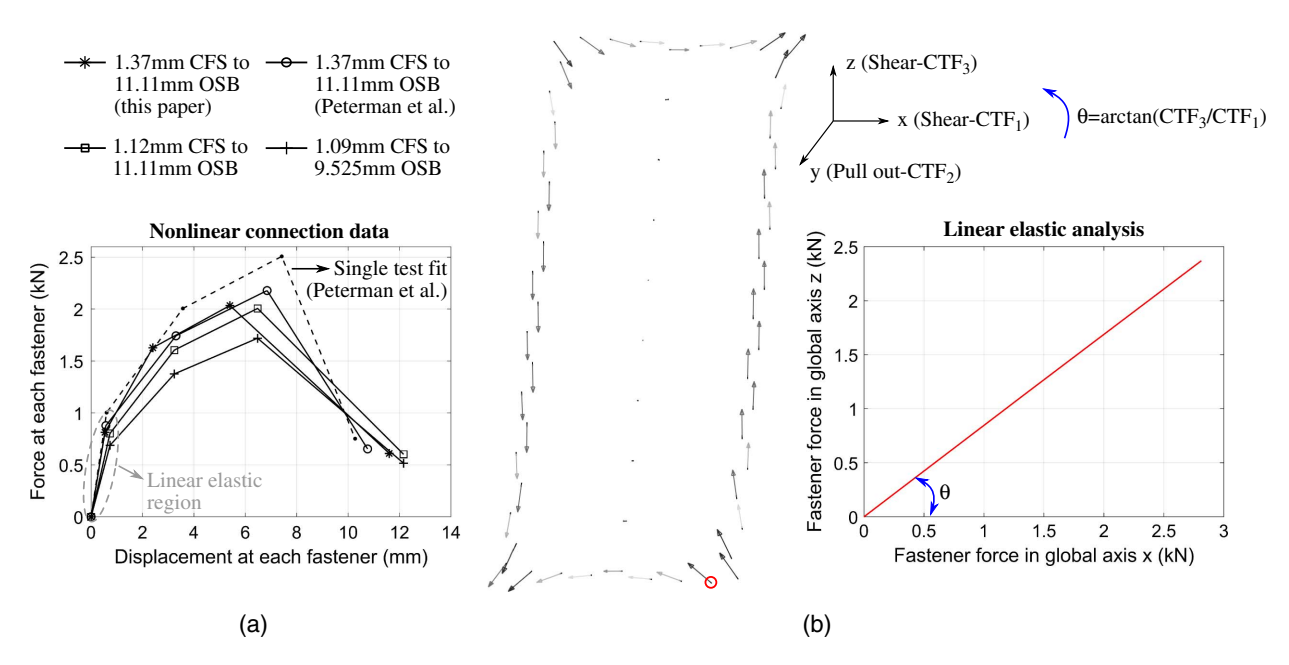


Fig. 6. CFS-to-OSB connection simulation: (a) nonlinear shear connection data adopted for the different examined CFS-to-OSB thickness combinations (solid lines = means used for FE model validation; and dashed line = single test fit to data used for a parametric analysis); and (b) vector forces and connection coordinate system angle calculation by implementing a linear elastic analysis. The CTF_1 is the total connection force at Direction 1 (x-axis), the CTF_2 is the total connection force at Direction 2 (y-axis), and the CTF_3 is the total connection force at Direction 3 (z-axis). The coordinate system is rotated about the out-of-plane Direction 2, aiming to a vector force alignment with the local shear Direction 1 at the top and bottom of the wall.

loading. The individual connection angles θ are then calculated from the connection force in shear axis z and the connection force in shear axis x (Fig. 6).

Stage B: A local coordinate system is introduced to each fastener as well as material, geometric, and connection nonlinearities, and a pushover analysis is performed. This aims to the alignment of the CFS-to-OSB connection vector forces to one of the two shear axes of the local coordinate system in order to avoid the excessive overestimation of the capacity of the connection during the analysis.

For the pull-out direction of CFS-to-OSB connections, a high stiffness of 1,750 kN/mm (10,000 kips/in.) is assumed in order to represent the negligible out-of-plane deformation of the OSB board. The pull-out direction of those connections is further discussed in the parametric analysis section of this paper.

CFS-to-CFS Connections

The connections between the cold-formed steel members (CFS-to-CFS connections), such as stud-to-stud, stud-to-track, and stud-to-ledger, were not observed to fail during the tests. For this purpose,

CFS-to-CFS connections are modeled by means of multipoint (MPC) pinned constraints, restraining the three translational degrees of freedom and allowing independent motion of the three rotational ones [Figs. 5(d and e)]. Stud-to-stud connections appear in the back-to-back chord studs, which are connected by two lines of connections with a 304.8 mm (12 in.) vertical spacing. Stud-to-track connections are simulated at the center points of the flanges between studs and tracks at the top and bottom of the wall, while the stud-to-ledger connections are modeled at the interior top side of the wall spacing 50.8 mm (2 in.) at each stud flange.

Boundary Conditions and Hold-Downs

Boundary conditions at the top and bottom of the wall are introduced based on the experimental configuration and rig of each CFS shear wall that is simulated in this study. An extensive description of the test rigs can be found in the experimental studies (Liu et al. 2014; Branston 2004; Blais 2006; Hikita 2006). At the bottom part of the wall, in all of the shear wall configurations examined in this paper, the bottom tracks are attached to the foundation by four

^aExperimentally-determined by Peterman et al. (2014).

shear anchors (two of them represent the shear anchors that are used in the hold-down positions), as shown in Fig. 5(g). In this case, pinned nodes are introduced in the locations of the shear anchors, and specifically, horizontal and out-of-plane directions are restrained (Directions 1 and 2 are restrained). At the top of the wall, two different categories of boundary conditions are introduced [Fig. 5(h)], as follows:

- Shear walls tested by Liu et al. (2014) are restrained in the outof-plane direction by restraining the translation in Direction 2.
 In this case, two lines of nodes with a 76.2-mm (3-in.) spacing
 are adopted based on the test rig and the location of the actuator.
- Shear walls tested by McGill University's setup (Branston 2004; Blais 2006; Hikita 2006) are restrained by one line of six shear anchors, which are modeled by restraining the wall out-of-plane movement (Direction 2 restrained) in the locations of the top rig bolts. The spacing between these bolts is 230 mm (9 in.).

Hold-downs are simulated by means of a rigid body at the bottom part of the wall. Specifically, a rigid body in the dimensions of the hold-downs is modeled in the chord stud webs tied to a reference point (RP) in the middle of it [Fig. 5(f)]. The reference point is connected to a fixed node at the ground by a linear SPRING2 element fixed in the vertical direction of the wall in order to prevent the uplift of the wall. Two types of hold-downs are modeled in this study: (1) a Simpson Strong-Tie S/HDU6; and (2) a Simpson Strong-Tie S/HD10 based on the experimental configurations tested by the CFS-NEES effort and the McGill work, respectively:

- For the S/HDU6 case, the stiffness of the hold-down attached to 1.37 mm (54 mils) CFS studs in tension is 2,929 kN/m (56.7 kips/in.), while the stiffness of the hold-down in compression is 1,000 times higher than the tension stiffness (Leng et al. 2013).
- For the S/HD10 case, the tensile stiffness is equal to 17,388 kN/m (99.3 kips/in.) for Branston (2004) and Blais (2006) walls because hold-downs are attached to 1.12 mm (44 mils) or 1.09 mm (43 mils) thick CFS studs and equal to 22,292 kN/m (127.3 kips/in.) for Hikita (2006) walls because hold-downs are attached to 1.37 mm (54 mils) studs. Likewise, the compressive stiffness is set to 1,000 times the tensile stiffness.

In both cases, hold-down dimensions and hold-down tensile stiffness is taken from the manufacturer using ASD predictions.

Interactions and Loading

Interactions are introduced between the cold-formed steel frame and oriented strand board sheathing (CFS-to-OSB components) as contact pairs by using surface-to-surface definitions. For CFS-to-OSB components, hard contact (normal behavior) is introduced between the flanges of studs and tracks with the OSB sheathing, while tangential behavior is not applied (friction coefficient varying between 0.2 and 0.6 is further discussed in the parametric analysis section). Penetration of the sheathing through the structural frame is eliminated through a master-slave definition in which the OSB sheathing is represented as the master surface (coarser mesh), and the stud and track flanges are the slave surface (finer mesh) in ABAOUS.

Monotonic loading is applied at the top of the simulated shear walls via displacement control. The cross-section of each top track is simulated as a rigid body tied to a reference point (RP) at the center of the track at which a displacement of 0.127 m (5 in.) (Liu et al. 2014) and 0.08 m (3 in.) (Branston 2004; Blais 2006; Hikita 2006) is applied [Fig. 5(i)]. The Newton-Raphson static method is used for the finite element analyses in this study by setting the initial time increment equal to 0.01, the minimum time

increment equal to 10^{-7} , and the maximum time increment equal to 0.01. A smaller initial and minimum time increment of 0.001 is also evaluated in the parametric analysis section.

Results and Discussion

The results of the experimental validation are presented in this study, followed by a reliability study on connection behavior and a sensitivity analysis on the impact of various shear wall parameters.

Experimental Validation of Computational Model

A comparison of the computational results with the experiments is provided in this study, emphasizing strength, stiffness, and failure modes.

Force-Displacement Response

Force-displacement curves for both experimental and computational results are shown in Fig. 7. The results illustrate that wall strength is accurately captured within 11% and in eight of the walls within 5% (Table 6). Furthermore, displacement at the peak load is captured within 5% in six of the examined walls (Branston 2004; Blais 2006) and within 23% in three of the walls (Liu et al. 2014; Hikita 2006). In six of the walls, three repetitions of the same test were conducted (denoted as experiment Nos. 1, 2, and 3 in Fig. 7), showing that a variance up to 11% exists between identical wall experiments for both the peak load and displacement at the peak load. The wall response variance through the finite element model is emphasized and further discussed in the following parametric analysis subsection. The postpeak wall response is out of the scope of this work.

The prepeak stiffness of the finite element model is characterized by three stiffness regions [Fig. 8(a)]. The stiffness region between Points O and A (between 0% and 40% model peak load) is denoted as the initial wall stiffness, the stiffness region between Points A and B (between 40% and 80% of the model peak load) is denoted as middle stiffness, and the stiffness region between Points B and C (between 80% and 100% of the model peak load) is denoted as the final stiffness. The results [Fig. 8(b)] show that stiffness of the wall is accurately captured when CFS-to-OSB connection behavior is informed by experimental data from the same test program, at which the sheathing and screws were identical with those tested in the shear walls (Liu et al. 2014) or when available experimental data based on the same CFS and OSB thickness are used (Hikita 2006), while the percentage difference is higher when the data interpolation of the CFS thickness is used (Branston 2004) and, specifically, when CFS and OSB thicknesses are both interpolated (Blais 2006). This observation highlights the importance of using experimentally-determined data for CFS-to-OSB connection behavior. This finding is enhanced by a reliability analysis following this subsection. The model secant stiffness between Points O and C [between 0% and 100% of the model peak load, as shown in Fig. 8(c)] is in agreement with the respective experimental secant stiffness, as illustrated in Fig. 8(d).

Although the purpose of this study is to compare the finite element modeling results to the experiments and not to compare the response of the different wall configurations with each other, Fig. 7 also demonstrates that the introduced modeling approach is able to capture the strength increase and stiffness decrease obtained by reducing the fastener spacing from 152.6 mm (6 in.) to 101.6 mm (4 in.) to 76.2 mm (3 in.) at the wall perimeter (Branston 2004; Blais 2006; Hikita 2006) and by increasing (double) the width of the wall (Liu et al. 2014).

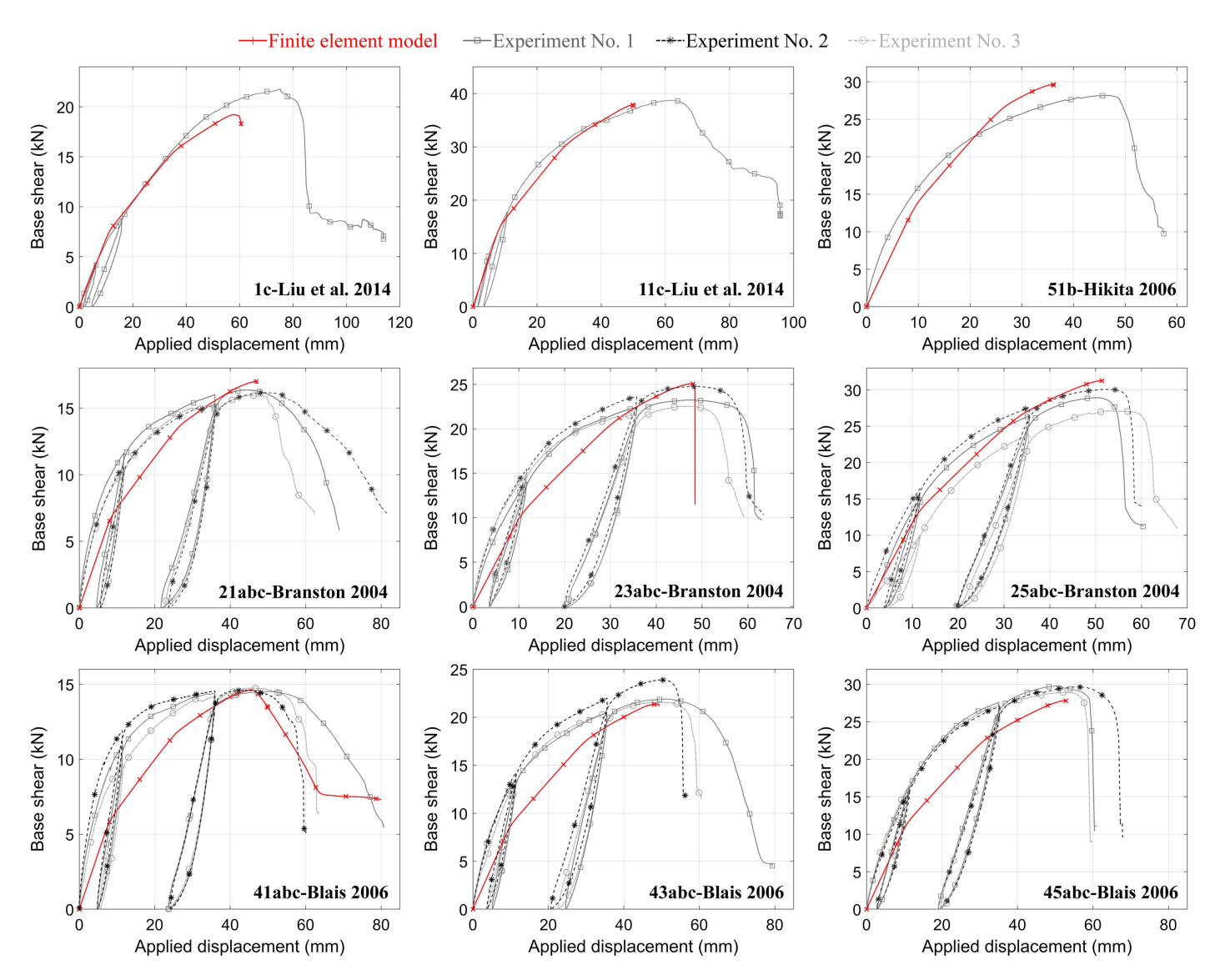


Fig. 7. Force-displacement response by nine different simulated shear wall configurations and a comparison with the available experimental test results. In the lower right of each plot is the specimen identifier from the corresponding work to which the finite element model is compared. The experiment number in the legend refers to the number of repetitions of the exact same test. The nine plots in this study illustrate the comparison between the numerical and experimental results; they are not intended for comparison with each other.

Table 6. Strength shear wall comparison between experiment, finite element model, and AISI S400-15 design code

CFS shear wall database (Test No.)	Experimental study (kN)	Computational model (kN)	AISI S400 code (kN)	Model difference ^a (%)	Code difference ^a (%)
Liu et al. (2014) (1c)	21.80	19.44	14.87	-11.90	-31.8
Liu et al. (2014) (11c)	38.73	38.17	33.45	-2.19	-13.6
Hikita (2006) (51b)	28.18	29.64	22.92	+5.18	-18.7
Branston (2004) (21abc)	16.36	17.01	12.07	+3.97	-26.2
Branston (2004) (23abc)	24.78	25.07	17.80	+1.17	-28.2
Branston (2004) (25abc)	30.09	31.28	22.92	+3.95	-23.8
Blais (2006) (41abc)	14.63	14.64	11.70	+0.07	-20.0
Blais (2006) (43abc)	21.59	21.39	17.43	-0.93	-19.3
Blais (2006) (45abc)	28.93	27.82	22.19	-3.84	-23.3
Overall				3.69	22.8
COV				1.11	4.4

Note: Percentage differences between computational and experimental results illustrate that wall strength is captured within 11% in all of the simulated cases. Strength overestimation is indicated by (+), and strength underestimation by (-).

^aIn comparison with experiments.

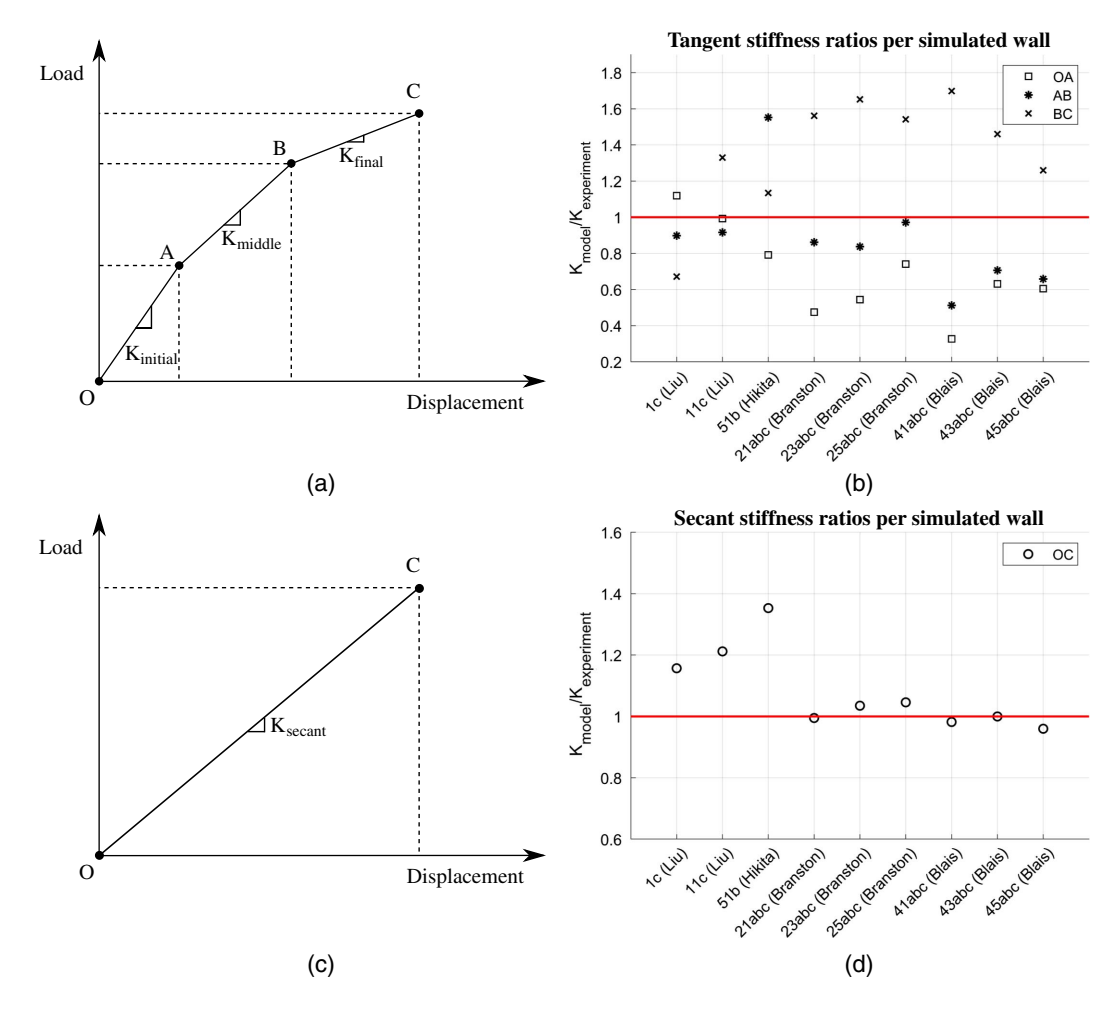


Fig. 8. Stiffness comparison between numerical and experimental results: (a) typical load-displacement curve illustrating the three different stiffness regions prepeak. Symbol *K* denotes the wall stiffness in the different regions. Region OA represents the initial stiffness of each simulated wall, region AB represents the end of the middle stiffness of each wall, and region BC represents the end of the final stiffness of each wall. Postpeak behavior of the wall is out of consideration in this study; (b) tangent stiffness ratios per tested specimen simulated in this study; (c) secant stiffness representation between Points O and C; and (d) secant stiffness ratios per tested specimen simulated in this study. This graph allows for comparisons between the different stiffness regions at each test, as well as for comparisons between the different tests for each stiffness region.

Failure Mechanisms

The governing failure mechanisms in all of the nine investigated shear wall configurations are fastener-based; the CFS-to-OSB connections fail during the computational analyses. This is in accordance with the experimental studies at which the shear screw failure and screw pull-through followed by the OSB bearing or OSB tear out to govern the overall shear wall response. The progression of the fastener failure is initiated by the corner fasteners and distributed to the immediate adjacent fasteners along the stud and track flanges in both the numerical and experimental studies. Fig. 9(d) demonstrates the force-displacement response of the CFSto-OSB fasteners at the bottom right part of the wall, and the progression of force transfer from one fastener to another. Although fastener failures are propagated from the wall corner fasteners, all of the four corners do not fail at the same time step. The failure is initiated by the bottom right corner of the wall, and it propagates to the bottom left part and, finally, to the top corners.

The local coordinate system of each fastener is shown in Fig. 9(b) [specimen 1c from Liu et al. (2014) wall is used for representation in this figure]. Before the peak load is reached, the vector forces maintain a constant angle during the analyses, which might alter in some of them after the wall peak load is reached.

Stress contours for section Point 1 are shown in Fig. 9(a); areas of high-stress concentration, located at the stud-to-track connections in accordance with the experiment, are shown in Fig. 9(c). Von Mises stresses increase up to the yielding point. Sheathing translates as a rotated rectangle, and small stress concentration is predicted.

Parametric Analysis

In this study, a sensitivity analysis of the many parameters (connections, material properties, mesh, contact, boundary conditions, hold-downs, and time step) inherent in shear wall modeling is conducted. As design codes [AISI S400-15 (AISI 2015)] are based primarily on strength, the peak strength is the basis of comparison between the models.

Reliability Analysis Focusing on the Variability of CFS-to-OSB Connections

The large inherent variability in the CFS-to-OSB connection response begets exploration of the impact of this variability on the shear wall strength and stiffness.

The 1.22×2.74 m (4 \times 9 ft) CFS shear wall [specimen 1c from Liu et al. (2014)] is used for this study, as the connection data available are well-established: the OSB and fasteners used in the shear

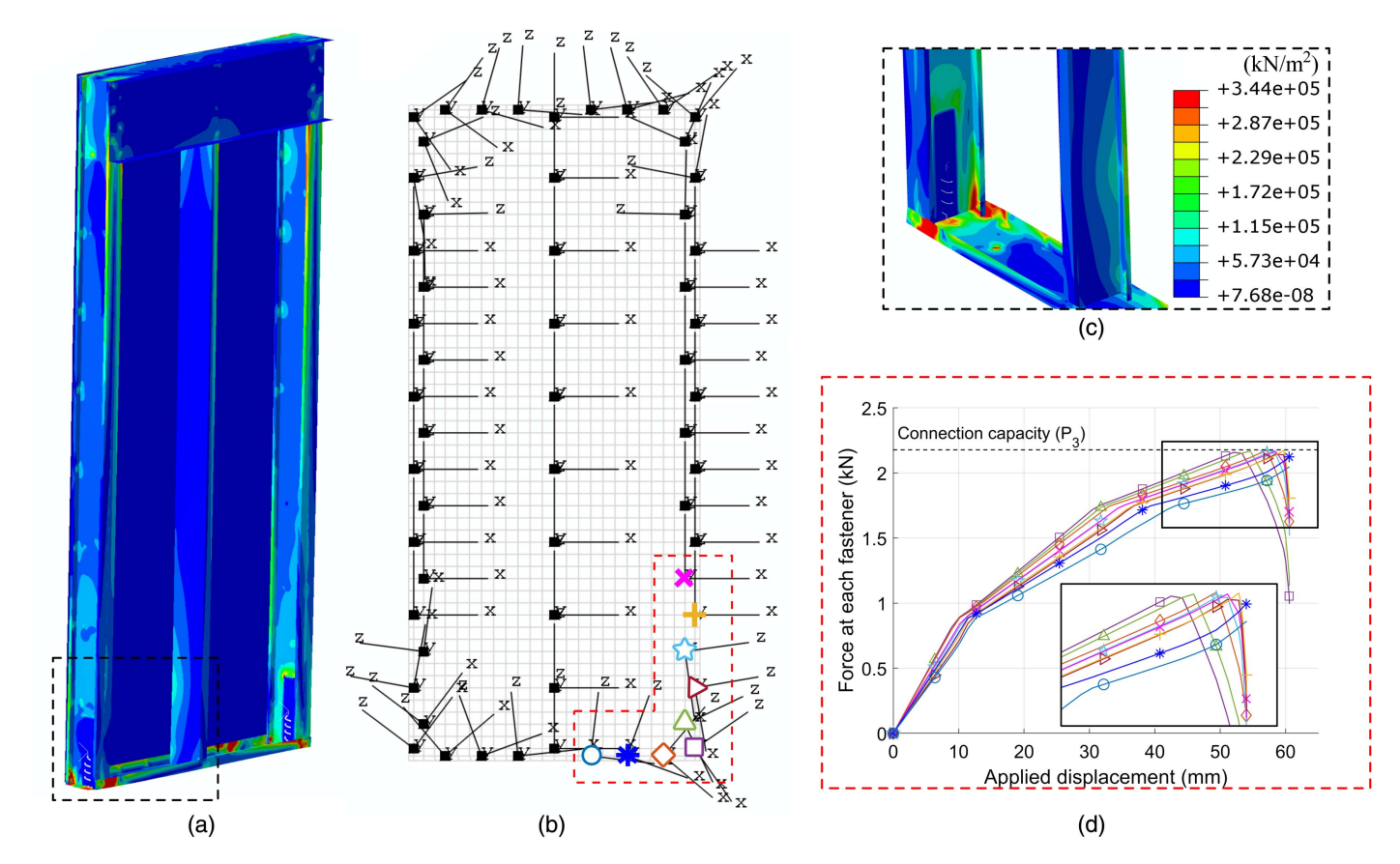


Fig. 9. Postprocessing model evaluation: (a) von Mises stress contours for section Point 1; (b) connection local coordinate system representation; (c) stress concentration close to stud-to-track connections; and (d) connection failure mechanisms representation at one of the wall corners. A zoom-in schematic of the connection forces at failure is included, illustrating the progression of failure with markers.

wall test program are identical with those in the fastener test program (Peterman et al. 2014). The connections tested in this study are nominally identical but are obviously sourced from different batches, separated from the 2014 experiments geographically and temporally. Thus, the Liu et al. (2014) shear wall was modeled three ways: (1) using the mean of the Peterman et al. (2014) data, shown in Fig. 6(a); (2) using the maximum recorded connection response from the Peterman et al. (2014) test program, shown in Fig. 6(b); and (3) using the mean of the nominally identical connection behavior determined in this paper, shown in Fig. 6(c). Even though the connection data are obtained by the same test rig, OSB thickness, CFS thickness, and screw-type and diameter in all the three cases, a wall variance of 16% is predicted between the finite element analyses. The results (Fig. 10) show not only the significant sensitivity of the introduced model by the CFS-to-OSB connection backbone behavior but also the importance of implementing the connection data that is from the same batch as the shear wall into the numerical model.

A more thorough statistical characterization of the shear wall response is obtained by introducing upper and lower wall bounds based on a $\mu \pm \sigma$ and $\mu \pm 2\sigma$ connection response from the 30-specimen experimental investigation described in a previous section. Using connection data within one standard deviation of the mean results in a variance in the peak strength of $\pm 12\%$, while data within two standard deviations result in a variance of $\pm 25\%$ [Fig. 10(d)]. The shaded regions represent the expected intermediate response range between the bounds. This analysis concludes that the proposed finite element model is highly sensitive to the CFS-to-OSB connection shear behavior.

Insensitivity Parameters of Computational Model

The proposed model response is also evaluated by examining the impact of different modeling parameters and assumptions. A parametric analysis focused on the strength effect is presented in this section (Table 7). The impact assessment is held by altering a unique parameter individually and maintaining the same remaining modeling parameters [comparison with the mean μ curve in Fig. 10(d)]. The positive sign (+) denotes a strength increase, while the negative sign (-) denotes a strength decrease in comparison with the statistical average response μ . For both, the strength increase and decrease by a specific parameter variation, (\pm) signs are used to describe the impact range from a negative to positive effect.

Specifically, the parameters that are examined in this study are as follows:

- The global CFS-to-OSB connection coordinate system, which increases the peak strength of the shear wall by 4.9% in comparison with a local coordinate system introduction at each fastener.
- The stiffness reduction in one of the CFS-to-OSB connection shear directions (Direction 3) varied between 0% and 100% of the initial connection stiffness, which decreases the strength of the wall between 2% and 4.4% in the examined range.
- The CFS-to-OSB pull-out direction stiffness varied between 1,506 kN/m (9 kips/in.) and 1,750,000 kN/m (10,000 kips/in.), which leads to a decrease of the wall peak load up to 0.61%.
- The stud-to-track connection Cartesian modeling by CFS-to-CFS experimental data (Tao et al. 2017), which reduces the wall peak load by a percentage of 3.5% in comparison with the MPC pinned constraint selection.

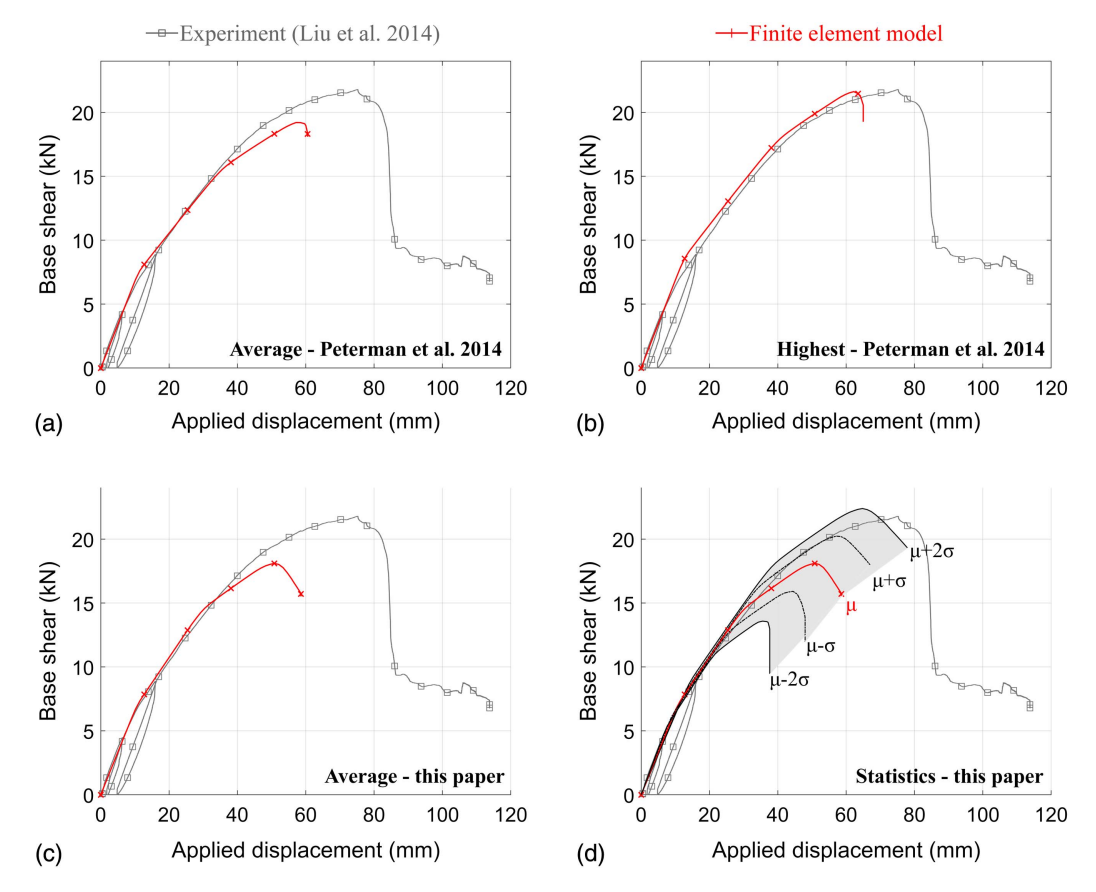


Fig. 10. CFS-to-OSB connection behavior impact in overall lateral shear wall response in comparison with the experiment [specimen 1c from Liu et al. (2014)]. Wall response by using 1.37 mm CFS to 11.11 mm OSB: (a) average connection data by Peterman et al. (2014); (b) highest capacity single test data by Peterman et al. (2014); (c) average connection behavior by the conducted 30 identical tests by this paper; and (d) higher and lower connection bounds based on a connection statistical characterization by this paper. The shaded area is the range of all possible responses within the bounds.

- The measured CFS material properties (thickness and yield strength), that increase the wall strength by 1.8% when compared to the wall response with nominal dimensions.
- The hold-down modeling by additionally restraining the web of the track as a rigid body, which leads to a strength increase of 1.3%.

Table 7. Parameter and assumption impact on the strength of OSB-sheathed CFS shear walls

Sensitivity/insensitivity parameters	Peak load impact (%)
CFS-to-OSB shear connection behavior	(±)25
Global connection coordinate system	(+)4.9
CFS-to-OSB shear stiffness in perpendicular	(-)2 to 4.4
local axis	, ,
CFS-to-OSB contact friction coefficient	(+)1.3 to 3.7
Stud-to-track connection Cartesian modeling	(-)3.5
CFS measured material properties	(+)1.8
Hold-down additional track rigid body	(+)1.3
modeling	, ,
CFS-to-CFS contact friction coefficient	(-)0.4 to 1
CFS-to-OSB pull-out connection behavior	(-)0.001 to 0.61
OSB sheathing modeling	(+)0 to 0.59
OSB mesh discretization	(+)0.57
Shear anchor modeling (BCs)	(+)0.02 to 0.19
OSB sheathing shear modulus	(+)0.03 to 0.09
Initial and minimum time increment	(+)0.04
Hold-down stiffness	(-)0.01 to $(+)0.02$

Note: Finite element model is primarily sensitive to CFS-to-OSB connection behavior.

- The hold-down stiffness varied between LRFD prediction 7,734 kN/m (41.8 kips/in.) and 17,388 kN/m (99.3 kips/in.), which affects the peak load by both an increase and decrease of 0.01%–0.02%. The percentage load decrease happens for a hold-down stiffness lower than 2,929 kN/m (56.7 kips/in.), while the load increase is predicted for higher hold-down stiffness.
- The CFS-to-OSB tangential contact definition by altering the friction coefficient between 0.2 and 0.6, which increases the peak strength of the wall between 1.3% and 3.7%.
- The CFS-to-CFS contact definition between the stud and track flanges presence by also altering the friction coefficient between 0.2 and 0.8, which affects the peak strength of the wall up to a 1% decrease.
- The OSB sheathing modeling as isotropic and/or plastic, which increases the peak load up to 0.59% in comparison with the elastic orthotropic material introduction.
- The OSB sheathing shear modulus varied between 1,316 MPa (191 ksi) and 10,000 MPa (1,450 ksi), which increases the peak load of the wall up to 0.09%.
- The smaller size mesh discretization of 38.1 mm (1.5 in.), which increases the strength of the wall by 0.57%.
- The shear anchors as fixed boundary conditions or pinned shear anchors excluding the hold-down anchors as boundaries in the bottom track, which leads to an increase up to 0.19% in comparison with all pinned-nodes bottom-track boundary conditions.
- The minimum and initial time increment of 0.001, which increases the strength of the wall by 0.04%, as well as the computational cost in comparison with a 0.01 time-increment.

The results illustrate that the impact of the aforementioned parameters in the CFS shear wall response is predicted to be very low, and specifically, less than a 5% difference is observed in all of the examined cases for those systems when compared to the wall response by using the 30-test average μ connection response. The shear wall stiffness is largely not impacted by any variable studied in this study except for the hold down stiffness and OSB shear modulus. When the hold-down stiffness varied from 2,929 kN/m (56.7 kips/in.) to 17,388 kN/m (99.3 kips/in.), and when the OSB shear modulus varied from 1,316 MPa (191 ksi) to 10,000 MPa (1,450 ksi), the shear wall stiffness [Point A in Fig. 8(a)] increased up to 19% in both cases. CFS-to-OSB connection data are observed to have the foremost effect in numerical CFS shear wall lateral response, as thoroughly discussed in the previous section. The shear connection response is additionally affected by environmental conditions, such as humidity, as studied by Vieira and Schafer (2009).

Comparison with Design Code

The shear wall experimental work cited in this paper contained detailed comparisons to the AISI design code (AISI S400-15) prescriptive methods and universally concluded that the code underpredicts the shear wall strength up to 32%. Because OSB-sheathed CFS shear walls are governed by a variable connection response, the code prediction for strength capacities based on a few test repetitions may be significantly divergent. The modeling suite detailed in this paper further validates this underprediction (Table 6) and motivates the recalibration of the existing prescriptive methods and expansion to shear walls not currently included.

Conclusions

The conclusions and the impact of this work are multifaceted in both CFS research and design code applications.

This study firstly quantifies the inherent and significant connection response variability between CFS components and OSB sheathing. The conducted 30-identical specimen experimental program shows that a 38% variability lies around the CFS-to-OSB connection shear behavior. Furthermore, two failure mechanisms govern the connection response: screw pull-through and shear screw failure. Localized sheathing bearing accompanies both failure modes.

Another important finding of this work lies in the efficacy of the fastener-based computational models to capture the OSB-sheathed CFS shear wall response and complex failure modes. Specifically, the introduced high-fidelity modeling approach is able to capture strength, stiffness, and fastener-oriented failure modes of different shear wall configurations when compared with nine different recent experimental studies. The key point of the proposed computational tool is the connection modeling, which recommends or necessitates experimental-determined connections data use for the CFS-to-OSB connection in order to capture the full shear wall response accurately.

A high percentage discrepancy of up to 25% is observed in the lateral wall response when connection data vary between μ and $\mu\pm2\sigma$. Any other examined modeling parameter and assumption is not predicted to significantly affect the estimated strength and accuracy of the proposed CFS shear wall model. Although the strength and failure modes only seem to be affected by the CFS-to-OSB connections, the wall stiffness is also affected by the hold-down stiffness and OSB shear modulus along with the connection behavior.

Finally, the proposed finite element model not only aims to fill the gap in the research community, but it is also intended to be used for design code expansion. The AISI S400 design code conservatively predicts the lateral shear capacity of the OSB-sheathed CFS shear walls, and its design applications are limited to specific component thicknesses and fastener patterns. For this reason, the validated computational tool can play a fundamental role in that direction.

This work is also intended to be used as a benchmark and to be expanded into different sheathing materials, such as steel, fiber cement boards, and sure-boards for both CFS shear walls and CFS diaphragm finite element modeling, with potential use on full building capacity predictions and design.

Data Availability Statement

Some or all data, models, or code generated or used during the study are available from the corresponding author by request. The data include the computational and experimental results and the experimental raw data.

Notation

The following symbols are used in this paper:

B = stud and track flange width (mm);

COV = coefficient of variation of connection response (%);

 CTF_1 = connection total force at Direction 1 in Abaqus;

 CTF_2 = connection total force at Direction 2 in Abaqus;

 CTF_3 = connection total force at Direction 3 in Abaqus;

H = stud and track web depth (mm);

D = stud and track lip depth (mm);

E = modulus of elasticity of CFS (MPa);

 E_s = modulus of elasticity of OSB sheathing (MPa);

 E_{s1} = modulus of elasticity of OSB sheathing // to strength axis (kN · mm²/mm);

 E_{s2} = modulus of elasticity of OSB sheathing \perp to strength axis (kN · mm²/mm);

 E_{s3} = out-of-plane panel modulus of elasticity of OSB sheathing (kN · mm²/mm);

 $(EI)_s$ = panel bending stiffness (kN · mm²/mm);

 G_s = shear modulus of OSB sheathing (MPa);

 G_{s12} = shear modulus of OSB sheathing through thickness (MPa);

 G_{s13} = out-of-plane shear modulus of OSB sheathing (MPa);

 G_{s23} = out-of-plane shear modulus of OSB sheathing (MPa);

 $(Gt)_s$ = panel rigidity (kN/mm);

h = shear wall height (m);

K = stud-screw-sheathing specimen stiffness (kN/m);

 K_i = individual screw stiffness (kN/m);

P = stud-screw-sheathing specimen force (kN);

 P_i = individual screw force (kN);

 P_1 = individual screw force at 40% peak load (kN);

 P_2 = individual screw force at 80% peak load (kN);

 P_3 = individual screw force at 100% peak load (kN);

 P_4 = individual screw force at 30% post peak load (kN);

s = screw spacing at stud-screw-sheathing tests (mm);

 s_p = screw spacing at shear wall perimeter (mm);

 s_f = screw spacing at shear wall field stud (mm);

 $t_1 = \text{stud thickness (mm)};$

 $t_2 = \text{track thickness (mm)};$

 t_s = sheathing thickness (mm);

- w =shear wall width (m);
- Δ = stud-screw-sheathing specimen displacement (mm);
- Δ_i = individual screw displacement (mm);
- Δ_1 = individual screw displacement at 40% peak load (mm);
- Δ_2 = individual screw displacement at 80% peak load (mm);
- Δ_3 = individual screw displacement at 100% peak load (mm);
- Δ_4 = individual screw displacement at 30% post peak load (mm);
- θ = connection local coordinate system angle calculation;
- μ = mean connection response (mm or kN);
- ν = Poisson's ratio of CFS;
- ν_s = Poisson's ratio of OSB sheathing; and
- σ = standard deviation of connection response (mm or kN).

References

- AISI (American Iron and Steel Institute). 2012. North American specification for cold-formed steel framing—General provisions. AISI S200-12. Washington, DC: AISI.
- AISI (American Iron and Steel Institute). 2015. North American standard for seismic design of cold-formed steel structural systems. AISI S400-15. Washington, DC: AISI.
- AISI (American Iron and Steel Institute). 2016. North American specification for the design of cold-formed steel structural members. AISI S100-16. Washington, DC: AISI.
- APA (The Engineered Wood Association). 2012. Panel design specification. APA-D510C. Tacoma, WA: APA.
- Bian, G., A. Chatterjee, S. G. Buonopane, S. R. Arwade, C. D. Moen, and B. W. Schafer. 2017. "Reliability of cold-formed steel framed shear walls as impacted by variability in fastener response." *Eng. Struct*. 142 (Jul): 84–97. https://doi.org/10.1016/j.engstruct.2017.03.072.
- Bian, G., D. Padilla-Llano, J. Leng, S. Buonopane, C. Moen, and B. Schafer. 2015. "Opensees modeling of cold-formed steel framed wall system." In *Proc.*, 8th Int. Conf. on Behavior of Steel Structures in Seismic Areas. Shanghai: Tongji Univ.
- Blais, C. 2006. "Testing and analysis of light gauge steel frame 9 mm OSB panel shear walls." M.Eng. thesis, Dept. of Civil Engineering and Applied Mechanics, McGill Univ.
- Branston, A. E. 2004. "Development of a design methodology for steel frame/wood panel shear walls." M.Eng. thesis, Dept. of Civil Engineering and Applied Mechanics, McGill Univ.
- Branston, A. E., C. Y. Chen, F. A. Boudreault, and C. A. Rogers. 2006. "Testing of light-gauge steel-frame-wood structural panel shear walls." *Can. J. Civ. Eng.* 33 (5): 561–572. https://doi.org/10.1139/l06-014
- Buonopane, S., G. Bian, T. Tun, and B. Schafer. 2015. "Computationally efficient fastener-based models of cold-formed steel shear walls with wood sheathing." *J. Constr. Steel Res.* 110 (Jul): 137–148. https://doi.org/10.1016/j.jcsr.2015.03.008.
- Chen, C. Y. 2004. "Testing and performance of steel frame/wood panel shear walls." M.Eng. thesis, Dept. of Civil Engineering and Applied Mechanics, McGill Univ.
- Ding, C. 2015. "Monotonic and cyclic simulation of screw-fastened connections for cold-formed steel framing." M.S. thesis, Dept. of Civil and Environmental Engineering, Virginia Tech.
- Fiorino, L., G. Della Corte, and R. Landolfo. 2007. "Experimental tests on typical screw connections for cold-formed steel housing." *Eng. Struct.* 29 (8): 1761–1773. https://doi.org/10.1016/j.engstruct.2006.09.006.
- Fiorino, L., O. Iuorio, and R. Landolfo. 2008. "Experimental response of connections between cold-formed steel profile and cement-based panel." In *Proc.*, 19th Int. Specialty Conf. on Cold-formed Steel Structures. Rolla, MO: Wei Wen Yu Center for Cold-Formed Steel Structures.
- Fiorino, L., V. Macillo, and R. Landolfo. 2017. "Experimental characterization of quick mechanical connecting systems for cold-formed steel

- structures." *Adv. Struct. Eng.* 20 (7): 1098–1110. https://doi.org/10.1177/1369433216671318.
- Fülöp, L. A., and D. Dubina. 2004. "Performance of wall-stud cold-formed shear panels under monotonic and cyclic loading. Part II: Numerical modelling and performance analysis." *Thin Walled Struct.* 42 (2): 339–349. https://doi.org/10.1016/S0263-8231(03)00064-8.
- Hikita, K. 2006. "Impact of gravity loads on the lateral performance of light gauge steel frame/wood panel shear walls." M.Eng. thesis, Dept. of Civil Engineering and Applied Mechanics, McGill Univ.
- Iuorio, O., L. Fiorino, and R. Landolfo. 2014. "Testing CFS structures: The new school BFS in Naples." *Thin Walled Struct.* 84 (Nov): 275–288. https://doi.org/10.1016/j.tws.2014.06.006.
- Kechidi, S., and N. Bourahla. 2016. "Deteriorating hysteresis model for cold-formed steel shear wall panel based on its physical and mechanical characteristics." *Thin Walled Struct*. 98 (Jan): 421–430. https://doi.org/10.1016/j.tws.2015.09.022.
- Leng, J., B. W. Schafer, and S. G. Buonopane. 2013. "Modeling the seismic response of cold-formed steel framed buildings: Model development for the CFS-NEES building." In *Proc.*, *Annual Stability Conf.-Structural Stability Research Council*. Chicago: Structural Stability Research Council, American Institute of Steel Construction.
- Liu, P., K. D. Peterman, and B. W. Schafer. 2012. Test report on cold-formed steel shear walls. Research Rep. No. CFS-NEES. Baltimore: Johns Hopkins Univ.
- Liu, P., K. D. Peterman, and B. W. Schafer. 2014. "Impact of construction details on OSB-sheathed cold-formed steel framed shear walls." J. Constr. Steel Res. 101 (Oct): 114–123. https://doi.org/10.1016/j .jcsr.2014.05.003.
- Martínez-Martínez, J., and L. Xu. 2011. "Simplified nonlinear finite element analysis of buildings with CFS shear wall panels." J. Constr. Steel Res. 67 (4): 565–575. https://doi.org/10.1016/j.jcsr.2010.12.005.
- Moen, C. D., F. Tao, and R. Cole. 2016. "Monotonic and cyclic backbone response of single shear cold-formed steel screw-fastened connections."
 In *Proc., Int. Specialty Conf. on Cold-Formed Steel Structures*. Rolla, MO: Wei Wen Yu Center for Cold-Formed Steel Structures.
- Ngo, H. H. 2014. "Numerical and experimental studies of wood sheathed cold-formed steel framed shear walls." M.S. thesis, Dept. of Civil and Systems Engineering, Johns Hopkins Univ.
- Okasha, A. F. 2004. "Performance of steel frame/wood sheathing screw connections subjected to monotonic and cyclic loading." M.Eng. thesis, Dept. of Civil Engineering and Applied Mechanics, McGill Univ.
- Peterman, K. D., N. Nakata, and B. W. Schafer. 2014. "Hysteretic characterization of cold-formed steel stud-to-sheathing connections." J. Constr. Steel Res. 101 (Oct): 254–264. https://doi.org/10.1016/j.jcsr.2014.05.019.
- Peterman, K. D., M. J. Stehman, R. L. Madsen, S. G. Buonopane, N. Nakata, and B. W. Schafer. 2016a. "Experimental seismic response of a full-scale cold-formed steel-framed building. I: System-level response." J. Struct. Eng. 142 (12): 04016127. https://doi.org/10.1061/(ASCE)ST.1943-541X.0001577.
- Peterman, K. D., M. J. Stehman, R. L. Madsen, S. G. Buonopane, N. Nakata, and B. W. Schafer. 2016b. "Experimental seismic response of a full-scale cold-formed steel-framed building. II: Subsystem-level response." J. Struct. Eng. 142 (12): 04016128. https://doi.org/10.1061/(ASCE)ST.1943-541X.0001578.
- Schafer, B. W., et al. 2016. "Seismic response and engineering of cold-formed steel framed buildings." In Vol. 8 of *Structures*, 197–212. Amsterdam, Netherlands: Elsevier.
- Schafer, B. W., Z. Li, and C. D. Moen. 2010. "Computational modeling of cold-formed steel." *Thin Walled Struct.* 48 (10–11): 752–762. https:// doi.org/10.1016/j.tws.2010.04.008.
- Schafer, B. W., R. H. Sangree, and Y. Guan. 2007. Experiments on rotational restraint of sheathing: Final report. Washington, DC: American Iron and Steel Institute.
- Serrette, R., J. Encalada, G. Hall, B. Matchen, H. Nguygen, and A. Williams. 1997a. Additional shear wall values for light weight steel framing. Rep. No. LGSRG-1-97. Santa Clara, CA: Santa Clara Univ.

- Serrette, R. L., J. Encalada, M. Juadines, and H. Nguyen. 1997b. "Static racking behavior of plywood, OSB, gypsum, and fiberbond walls with metal framing." *J. Struct. Eng.* 123 (8): 1079–1086. https://doi.org/10 .1061/(ASCE)0733-9445(1997)123:8(1079).
- Serrette, R. L., K. A. Morgan, and M. A. Sorhouet. 2002. Performance of cold-formed steel-framed shear walls: Alternative configurations. Final Rep. No. LGSRG-06-02. Santa Clara, CA: Santa Clara Univ.
- Serrette, R. L., H. Nguyen, and G. Hall. 1996. *Shear wall values for light weight steel framing*. Rep. No. LGSRG-3-96. Santa Clara, CA: Santa Clara Univ.
- Tao, F., A. Chatterjee, and C. D. Moen. 2017. Monotonic and cyclic response of single shear cold-formed steel-to-steel and sheathing-to-steel connections. Rep. No. CE/VPI-ST-16-01. Blacksburg, VA: Virginia Tech.
- Vieira, L., and B. W. Schafer. 2009. "Experimental results for translational stiffness of stud-sheathing assemblies." In AISI-COFS project on sheathing braced design of wall studs. Baltimore: Johns Hopkins Univ.
- Vieira, L. C. M., Jr., and B. W. Schafer. 2012. "Lateral stiffness and strength of sheathing braced cold-formed steel stud walls." *Eng. Struct.* 37 (Apr): 205–213. https://doi.org/10.1016/j.engstruct.2011.12.029.